Adiabatic modulation of a superconducting quantum interference device (SQUID) ring by an electromagnetic field

1998 J. Phys.: Condens. Matter 10 9951

(http://iopscience.iop.org/0953-8984/10/44/004)

J. Phys.: Condens. Matter **10** (1998) 9951–9968. Printed in the UK PII: S0953-8984(98)87576-0

Adiabatic modulation of a superconducting quantum interference device (SQUID) ring by an electromagnetic field

R Whiteman, V Schöllmann, M Everitt, T D Clark†, R J Prance, H Prance, J Diggins, G Buckling and J F Ralph

Physical Electronics Group, School of Engineering, University of Sussex, Brighton BN1 9QT, Sussex, UK

Received 12 September 1997, in final form 1 September 1998

Abstract. In this paper we consider the modulation of a SQUID ring (a Josephson weak link enclosed by a thick superconducting ring) by an external electromagnetic (em) field for the case where the ring remains adiabatically in its ground state. We demonstrate that very good agreement can be found between experimental modulation data and the results predicted theoretically by solving the time-dependent Schrödinger equation for the ring–em-field system. We also show that the non-linear dynamical coupling between the ring and an external resonant circuit can influence the exact form of the modulation. Again we find consistent agreement between experiment and theory.

1. Introduction

Over the last decade or so the macroscopic quantum mechanical behaviour of SQUID rings (in this work, a single Josephson weak link enclosed by a thick superconducting ring) has been the subject of much research [1–4]. Although this is just one of the two basic types of SQUID ring (the other, the so-called DC SQUID, consisting of two Josephson weak links in parallel in a thick superconducting ring structure), its quantum description is straightforward. Thus, unlike the DC SQUID, the single-weak-link SQUID ring is not coupled to an external, incoherent source of current which, to our knowledge, has still to be dealt with in any adequate fashion quantum mechanically. It is also clear that one weak link in a superconducting ring is the simplest bound potential problem that we can deal with in the macroscopic quantum behaviour of SQUID rings.

Within this general field of interest we have recently considered the problem of electromagnetically induced quantum transitions between SQUID ring energy levels. This has required us to solve the time-dependent Schrödinger equation (TDSE) for a SQUID ring in an electromagnetic (em) field. To make the problem tractable we have restricted ourselves to considering em fields with free-space wavelengths large compared with the size of the SQUID ring [5]. For the niobium SQUID rings that we have actually used in experiment (a few mm in diameter) this means em frequencies ν_{em} in the microwave range (say, a few to 10 GHz). Furthermore, for ultralow-capacitance SQUID rings of this size, the characteristic ring frequencies (i.e. the separation in frequency units between the ring eigenenergies) are

† E-mail: t.d.clark@sussex.ac.uk.

0953-8984/98/449951+18$19.50

typically large compared to ν_{em}, i.e. a few hundred GHz compared to a few GHz. This has made finding accurate solutions for the system TDSE computationally very demanding. Even so, we have been able to calculate the time-averaged expectation values of the ring energies as a function of the applied static (or quasi-static) magnetic flux Φ_{xqstat}. In passing, we note that the SQUID ring in an em field shares common ground with a range of similar problems in quantum optics [6].

As we have found [7, 8], there are two features of this time-dependent system which are of great interest. First, in relatively weak em fields the system can display highly non-perturbative behaviour, i.e. coherent multiphoton absorption processes tend to be the rule. This is because the strength of the interaction between the ring and the em field ($\cong\Phi_{em}^2/2\Lambda$, where Φ_{em} is the magnetic flux amplitude of the field) can easily be comparable with the spacing between the original eigenenergies of the ring, even when Φ_{em} is only a fraction of a flux quantum Φ_0 ($=h/2e$). Second, regions of contact are found between adjacent solutions (the time-averaged energy levels) of the system TDSE at particular values of Φ_{xqstat}. These contact regions are to be identified with quantum transitions in the ring, generally involving multiphoton absorption. For microwave frequencies, and typical SQUID parameters, the spacing between these transition regions is on the scale of one to a few $\times 10^{-3}\Phi_0$ in Φ_{xqstat}, while their widths are an order of magnitude smaller ($\simeq 10^{-4}\Phi_0$). These calculations show that the strong coupling between the SQUID ring and the em fields does allow transitions to occur between energy levels at field frequencies much lower than indicated by the energy level separation. Therefore, it would be possible for thermal fluctuations to excite single- or multiphoton resonances. However, two factors are likely to suppress any thermally driven excitations. The superconducting shield used to enclose the SQUID rings used in the experiments described in this paper, and the superconducting rings themselves, do not form simple black-body cavities. It is unlikely, therefore, that the number of modes available in such hybrid cavities will have the same frequency distribution as a black body. The likelihood that the cavities used in the experiments (approximately a few centimetres across) will have significant numbers of long-wavelength modes at the frequencies required for resonance is small. In addition, at 4.2 K any cavity modes that are present will tend to have very small field energies (i.e. low photon numbers/amplitudes). Since the apparent widths of the multiphoton transitions are highly dependent on the amplitude of the applied field, the combination of limited long-wavelength cavity modes and small field amplitudes makes it very unlikely that thermally driven excitations play a significant role in the experiments described in this paper. Experimental resolution of the contact regions still appears to be just beyond the capabilities of currently available electronic techniques. Nevertheless, we have recently reported experimental data which provide supporting evidence for their existence [9]. Within the limits imposed by our electronics we appear to be observing clusters of these transition regions spreading over ranges in Φ_{xqstat}, rather than individual transitions.

These experimental data were collected using a radio-frequency (rf) reactive technique which we have refined over the years [10]. In principle this is very simple; the SQUID ring is inductively coupled to a rf parallel resonant (tank) circuit [11, 12] and the coupled system is probed using a rf signal of very small amplitude, typically a very small fraction of a Φ_0. Any rapid change in ring energy with external applied flux creates a correspondingly rapid change in the supercurrent circulating in the ring. This, in turn, generates non-linear dynamical behaviour in the coupled rf tank circuit which, of course, can be followed experimentally. Since it is the quantum evolution of the SQUID ring (through the screening current) which creates the non-linear dynamics in the tank circuit, this dynamics can be used to infer the underlying quantum behaviour of the ring. For example, we can use this dynamics to infer the lowest-lying, external-flux-dependent energy eigenvalues of the ring.

The small-amplitude dynamics of ring–tank-circuit systems is complemented in practice by the well known large-amplitude ($\simeq$a few Φ_0) SQUID magnetometer characteristics where the rf voltage $V_{\rm out}$ across the tank circuit is plotted against the input rf drive current $I_{\rm in}$.

The rf reactive technique can be used to probe both adiabatic and non-adiabatic behaviour of a SQUID ring in an em field. As we have demonstrated by computation [7, 8], adiabatic behaviour, with the ring remaining in its ground state, should be observed when the em frequency and/or amplitude is sufficiently small. In the non-adiabatic case, at sufficiently higher frequencies and/or amplitudes, transition regions may develop with a spacing in $\Phi_{\rm xqstat}$ determined by $\nu_{\rm em}$. For the circuit parameter values typical of the point contact SQUID rings that we have investigated (with a minimum separation between the lowest two eigenenergies of around 200 GHz in frequency units), the computed changeover between adiabatic and non-adiabatic behaviour starts at frequencies of a few GHz. This appears to be seen experimentally. Clearly, in any programme for probing quantum transitions in SQUID rings using rf reactive techniques it is essential that the adiabatic interaction of a SQUID ring with a monochromatic em field be first understood and recognized, both as regards computation and experiment. This adiabatic regime is the focus of the work described here.

2. Adiabatic modulation

We first consider the behaviour of a SQUID ring in terms of the time-independent Schrödinger equation (TISE). We take the geometric inductance of the ring, and the effective capacitance of the weak link enclosed by it, to be Λ and C, respectively. The eigenenergies $E_\kappa(\Phi_{\rm x})$ of the ring ($\kappa = 0$, ground state; $\kappa = 1$, first excited state etc), Φ_0-periodic in the applied flux $\Phi_{\rm x}$, can be found by solving the TISE [1, 2]

$$H(Q, \Phi, \Phi_{\rm x})\Psi(\Phi, \Phi_{\rm x}) = E_\kappa(\Phi_{\rm x})\Psi(\Phi, \Phi_{\rm x}) \tag{2.1}$$

in the presence of an external magnetic flux $\Phi_{\rm x}$. Here, the conjugate electromagnetic field variables for the ring are Φ, the total magnetic flux in the ring, and Q, the total electric displacement flux at the weak link, where Φ and $Q \rightarrow -{\rm i}\bar{h}\,\partial/\partial\Phi$ play analogous roles to position and momentum, respectively. Thus, $[\Phi, Q] = {\rm i}\bar{h}$, with the implied uncertainty relation $\Delta\Phi\,\Delta Q \geqslant \bar{h}/2$. In the work reported here we are concerned with the regime in which $\Delta\Phi < \Phi_0, \Delta Q > 2e$, termed by us the flux mode from the Φ_0-periodicity of its behaviour. In this mode the ring Hamiltonian can be written as the sum of three terms (capacitive, inductive and Josephson phase-coherent coupling) and takes the form

$$H(Q, \Phi, \Phi_{\rm x}) = \frac{Q^2}{2C} + \frac{(\Phi - \Phi_{\rm x})^2}{2\Lambda} - \bar{h}\nu\cos\left(2\pi\frac{\Phi}{\Phi_0}\right) \tag{2.2}$$

where $\bar{h}\nu/2$ is the matrix element for coherent Josephson pair tunnelling through the weak link (the critical current $I_{\rm crit} = 2e\nu$). This Hamiltonian has been derived as a limiting case of a more general quantum electrodynamic description for the SQUID ring where both the electromagnetic field and the superconducting condensate in the ring are treated quantum mechanically [11]. We note that there is another regime of SQUID ring behaviour, quantum mechanically conjugate to the flux mode, which we term the charge mode. Here, $\Delta Q < 2e, \Delta\Phi > \Phi_0$, leading to voltage-periodic ($2e/C$) rather than flux-periodic (Φ_0) behaviour.

The SQUID rings used by us to investigate the adiabatic interaction were of the Zimmerman niobium point contact (microbridge constriction) type [12], displaying small critical currents ($\sim$a few μA). Point contact weak links in general have extremely small cross-sectional dimensions, typically of the order of the pair size. However, the actual

problem of estimating the effective capacitance of such weak links is not simple. In a recent series of articles [5, 13, 14] we have developed a fully quantum electrodynamic (QED) approach to the effective capacitance of the weak link in superconducting rings, taking the link (condensate) self-capacitance, the SQUID block capacitance and the transverse (flux-tunnelling) capacitance all into consideration. We find that in this QED analysis the weak-link self-capacitance ($\simeq$a few 10^{-17} F for weak-link spatial dimensions close to 0.1 μm, weak-link critical currents of a few μA and Fermi velocities in niobium of around 10^6 m s^{-1}) is in series with the block capacitance ($\simeq 10^{-12}$ F for our block dimensions), with this series combination in parallel with the transverse capacitance (also around 10^{-16} F for our block dimensions). The resultant overall capacitance of the SQUID ring is close to 10^{-16} F. This appears to be borne out by the many experiments that we have performed on niobium point contact SQUID rings in both the flux and charge mode regimes [10, 15]. Dealing with the value of the geometric inductance Λ of the SQUID ring is much easier. For a two-hole Zimmerman ring this has been found (i) by direct measurement of the resonant frequency of the ring with no point contact weak link in place and (ii) by calculation [16]. Both methods yield an inductance very close to that quoted in this work (3×10^{-10} H).

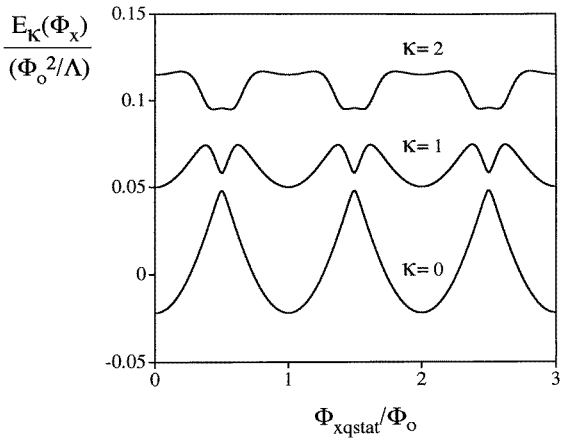

Figure 1. The first three flux-dependent eigenenergies found by solving the TISE for the SQUID parameters $\bar{h}\nu = 0.06\Phi_0^2/\Lambda$ and $\bar{h}\omega_0 = 0.043\Phi_0^2/\Lambda$ with $\Lambda = 3 \times 10^{-10}$ H.

To illustrate the form of the flux mode eigenenergies, and using the values of C ($=10^{-16}$ F) and Λ (3×10^{-10} H), discussed in the previous section, we show in figure 1 the first three levels ($\kappa = 0, 1$ and 2) where we have taken $\bar{h}\nu = 0.06\Phi_0^2/\Lambda$, corresponding to a weak-link critical current $I_{crit} = 2.5$ μA. As can be seen, the minimum energy difference (splitting) $(\Delta E_{01})_{min}$ between the $\kappa = 0$ and 1 states occurs at $\Phi_x = (n+1/2)\Phi_0$, n integer. What is also apparent is that where $(\Delta E_{01})_{min} \ll \bar{h}/\sqrt{\Lambda C}$ (as it is in this example) this minimum splitting is always much smaller than the minimum gaps between the $\kappa = 1$ and 2 levels. This relatively very small minimum splitting sets the precise form of the $\kappa = 0$ and 1 states. Given this small splitting, the nature of the quantum mechanical ground state ($\kappa = 0$) is apparent. This ground state comprises a superposition of the progenitor discrete flux states $n\Phi_0$, n integer, of the thick superconducting ring without a weak link. These progenitor states would be the parabolic sections of the $\kappa = 0$ energy $E_0(\Phi_x)$ in figure 1. The weak link allows flux tunnelling into and out of the ring, provided the link section is comparable with the superconducting penetration depth. This tunnelling acts

quantum mechanically to create (to lowest order) superpositions of nearest-neighbour flux states (e.g. $n\Phi_0 \rightarrow (n \pm 1)\Phi_0$) with coefficients which are determined by the external flux applied (modulo Φ_0). Equal-amplitude superpositions occur at the half-integer static bias fluxes $\Phi_{\mathrm{xqstat}} = (n + 1/2)\Phi_0$.

With regard to the response of a SQUID ring to an external applied flux, the important physical quantities are the expectation value of the screening supercurrent flowing around the ring

$$\langle I_{\mathrm{s}}(\Phi_{\mathrm{x}})\rangle_\kappa = -\partial E_\kappa(\Phi_{\mathrm{x}})/\partial\Phi_{\mathrm{x}} \tag{2.3}$$

and its derivative with respect to the external applied flux, the ring magnetic susceptibility

$$\chi_\kappa = \Lambda\,\partial\langle I_{\mathrm{s}}(\Phi_{\mathrm{x}})\rangle_\kappa/\partial\Phi_{\mathrm{x}}. \tag{2.4}$$

As we have already stated, this screening current is almost invariably probed via an inductively coupled tank circuit with a resonant frequency which is usually at rf ($\simeq$20 MHz) but may extend up to uhf (400 MHz) or beyond. The (non-linear) equation of motion for the coupled system is [17]

$$C_{\mathrm{t}}\ddot{\varphi} + \frac{\dot{\varphi}}{R_{\mathrm{t}}} + \frac{\varphi}{L_{\mathrm{t}}} = I_{\mathrm{in}}(t) + \mu\langle I_{\mathrm{s}}(\mu\varphi + \Phi_{\mathrm{xqstat}})\rangle_\kappa \tag{2.5}$$

where C_{t} and L_{t} are the capacitance and inductance, respectively, of the tank circuit, R_{t} is its resistance at parallel resonance, φ is the high-frequency flux (rf or otherwise) in the tank-circuit coil, μ is the fraction of flux coupling between the tank-circuit coil and the ring, $I_{\mathrm{in}}(t)$ is the time-dependent current (rf monochromatic and/or noise) driving the tank circuit and Φ_{xqstat} is the static bias flux applied to the ring. In general, for arbitrary coupling, the resonance lineshape (including the peak frequency $f_{\mathrm{r}\kappa}$ and peak amplitude $A_{\mathrm{r}\kappa}$) of this system must be found by solving the full non-linear equation of motion (2.5). However, for very weak coupling, and in the small-rf-oscillation limit ($|\varphi| \ll \Phi_0$), the resonant frequency can be approximated by linearizing (2.5) to yield [1, 10]

$$f_{\mathrm{r}\kappa} = \frac{f_{\mathrm{R}}}{\sqrt{1 + K^2\chi_\kappa(\Phi_{\mathrm{xqstat}})}} \tag{2.6}$$

where $f_{\mathrm{R}} = 1/2\pi\sqrt{L_{\mathrm{t}}C_{\mathrm{t}}}$ is the resonant frequency of the bare tank circuit and $K^2 = M^2/L_{\mathrm{t}}\Lambda = \mu^2 L_{\mathrm{t}}/\Lambda$, for a ring–tank-circuit-coil mutual inductance of M. Clearly, the form of (2.6) allows us to determine (through $\chi_\kappa \propto \partial^2 E_\kappa(\Phi_{\mathrm{x}})/\partial\Phi_{\mathrm{x}}^2$) whether the ring is in its ground state or in some low-lying excited state. For example, in the ground state, with no em modulation, the frequency shift pattern comprises a set of sharp, downward spikes set at Φ_0-intervals in Φ_{xqstat}. This is, in fact, our experimental test for the ring being in the ground state. Even within the solutions $E_\kappa(\Phi_{\mathrm{x}})$ of the TISE (2.1), the first, and subsequent, excited eigenstates ($\kappa = 0, 1$, etc) generate very different frequency shift patterns from the ground state [1].

We now consider the case of a quantum mechanical SQUID ring subject to a time-varying em field of the form $\Phi_{\mathrm{x}}(t) = \Phi_{\mathrm{xqstat}} + \Phi_{\mathrm{em}}\sin(\omega_{\mathrm{em}}t)$. Subject to the unitary transform $U = \exp(-\mathrm{i}\Phi_{\mathrm{x}}Q/\hbar)$ the TDSE for the ring takes the form [7, 8]

$$\left(\frac{Q^2}{2C} + \frac{\Phi^2}{2\Lambda} - \hbar\nu\cos\left(\frac{2\pi}{\Phi_0}[\Phi + \Phi_{\mathrm{x}}]\right) - Q\frac{\partial\Phi_{\mathrm{x}}}{\partial t}\right)|\psi\rangle = \mathrm{i}\hbar\frac{\partial|\psi\rangle}{\partial t}. \tag{2.7}$$

In this paper we are concerned with the situation in which the frequency and amplitude of the em field are sufficiently low that the ring remains in its ground state with no mixing in (superpositions) of higher states. This requires that $\partial\Phi_{\mathrm{x}}/\partial t$ be sufficiently small with respect to the other terms in equation (2.7) that it can be ignored. Under this constraint, the

adiabatic evolution operator [18, 7, 8] of the system is a diagonal matrix, and the SQUID ring does indeed remain adiabatically in its initial state. We are thus interested in the case where the ring is prepared in its ground state and remains adiabatically in this state even in the presence of an external em field. In this situation adiabaticity is maintained provided that

$$\frac{\partial \Phi_x}{\partial t} \ll \frac{1}{\hbar}(\Delta E_{01})_{\Phi_x=(n+1/2)\Phi_0}$$

which, in frequency-equivalent terms, is the minimum $\kappa = 0$ to 1 splitting. As we have recently shown [8], this assumption can be validated by solving (2.7) in the adiabatic limit. For the frequency separations between the ground and first excited eigenenergies considered in this paper (see figure 1), and for the em frequencies and flux amplitudes used in experiment, we have demonstrated by solving the TDSE for the system that only the ground state is modulated; there is no mixing in of contributions from higher states. The instantaneous (ground-state) energy of the ring can then be written as

$$E(t) = E_0(\Phi_{\text{xqstat}} + \Phi_{\text{em}} \sin(\omega_{\text{em}} t)). \tag{2.8}$$

Our interest is, of course, in the response of the tank circuit coupled to the SQUID ring. Provided that $\omega_{\text{em}}/2\pi \gg f_R$ (and $1/Q \ll 1$), which are the conditions found in our experiments, then the tank circuit is not directly driven by the em field but sees the average screening current in the ring as it is modulated. For the ground eigenstate ($\kappa = 0$) this average over one period of the external field takes the form

$$\overline{\langle I(\Phi_{\text{xqstat}})\rangle}_0 = \frac{\omega_{\text{em}}}{2\pi} \int_{-\pi/\omega_{\text{em}}}^{+\pi/\omega_{\text{em}}} I_0(\Phi_{\text{xqstat}} + \Phi_{\text{em}} \sin(\omega_{\text{em}} t))\ \mathrm{d}t. \tag{2.9}$$

In turn, the average, or modulated, adiabatic magnetic susceptibility of the ring $\overline{\chi_0(\Phi_{\text{xqstat}})}$ is given by

$$\overline{\chi_0(\Phi_{\text{xqstat}})} = \frac{\partial \overline{\langle I(\mu\varphi + \Phi_{\text{xqstat}})\rangle}_0}{\partial \Phi_{\text{xqstat}}}. \tag{2.10}$$

The periodicity of the eigenstates of the SQUID ring means that it is possible to express each of the states (and their derivatives) by Fourier series

$$E_\kappa(\Phi_x) = \frac{a_0^\kappa}{2} + \sum_{n=1}^{\infty} a_n^\kappa \cos\left(2n\pi \frac{\Phi_x}{\Phi_0}\right) \tag{2.11}$$

for which the coefficients a_n^κ can be calculated very rapidly. This representation enables us to perform the averaging integral (2.9) above analytically and it follows that

$$\overline{\chi_0(\Phi_{\text{xqstat}})} = \sum_{n=1}^{\infty} a_n^0 (2n\pi)^2 \cos\left(2n\pi \frac{\Phi_{\text{xqstat}}}{\Phi_0}\right) J_0\left(2n\pi \frac{\Phi_{\text{em}}}{\Phi_0}\right). \tag{2.12}$$

Here, we see that the modulated susceptibility $\overline{\chi_0(\Phi_{\text{xqstat}})}$ has a J_0 Bessel function dependence as will be apparent in the experimental data presented in this paper.

3. Experimental technique

To follow $\chi_0(\Phi_{\text{xqstat}})$ we used the rf reactive technique [1, 10], assuming the weak coupled approximation, after (2.6). The tank circuit, coupled to the SQUID ring, was excited by means of a small-amplitude current source (corresponding to a flux amplitude at the ring in the range $\Phi_0/50$ to $\Phi_0/100$). At some fixed value of Φ_{xqstat} this constant-amplitude current

source was swept in frequency across the width of the ring–tank-circuit resonance. The peak frequency f_{r0} and peak amplitude A_{r0} of this resonance were recorded, Φ_{xqstat} was then incremented by approximately $\Phi_0/100$ and the measurement process repeated. This cycle was repeated many times in order to make plots of f_{r0} and A_{r0} over a number of Φ_0-periods in Φ_{xqstat}. With these patterns recorded, the screening current response $\langle I_s(\Phi_x)\rangle_0$ in the absence of em modulation could be inferred, either through (2.6) or through solutions of (2.5). Furthermore, the lineshape of $f_{r0}(\Phi_{xqstat})$ about $\Phi_{xqstat} = (n + 1/2)\Phi_0$ allowed us to estimate the energy separation $(\Delta E_{01})_{min}$. We note again that when $(\Delta E_{01})_{min} \ll \hbar/\sqrt{\Lambda C}$, we can also infer the form of the $\kappa = 0$ and 1 levels $E_0(\Phi_x)$ and $E_1(\Phi_x)$.

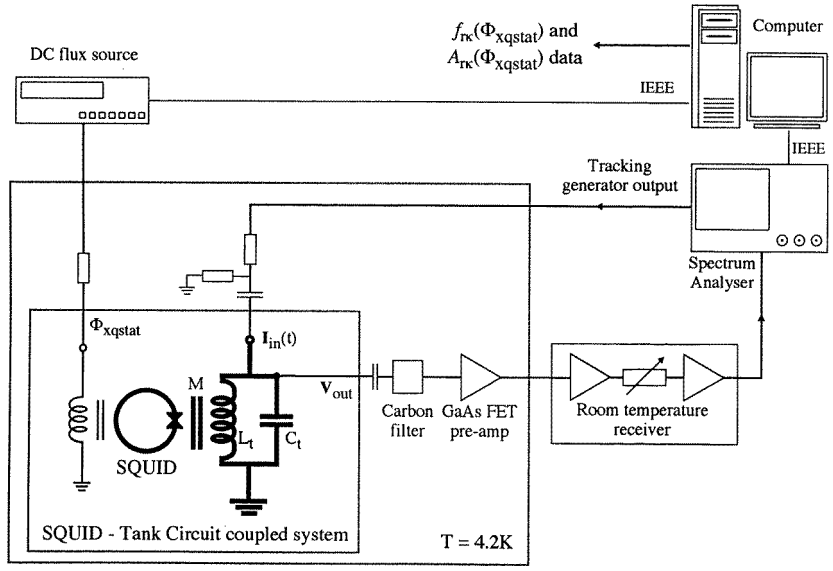

Figure 2. A block diagram of the cryogenic SQUID assembly, room temperature receiver system and spectrum analyser.

In practice the system resonance for each value of Φ_{xqstat} was recorded using a Rohde and Schwarz FSAS spectrum analyser operating under National Instruments LabVIEW virtual instrument software [19]. In addition, this analyser provided the variable-frequency, constant-amplitude rf excitation current used in our reactive probing. The voltage response of the tank circuit to this excitation current was first preamplified by means of a GaAs FET amplifier at 4.2 K, subsequent amplification and detection being achieved by means of a low-noise room temperature receiver of our own design. The block diagram for the low-temperature SQUID assembly and the experimental electronics is shown in figure 2. As mentioned earlier, the SQUID rings used in the experiments reported in this paper were of the Zimmerman niobium point contact type with weak-link critical currents in the few μA range. In experiment, the point contact in these ring structures was adjusted, *in situ*, at liquid helium temperatures.

In setting up SQUID rings (i.e. by adjusting the point contact in the ring), the large-amplitude dynamical (V_{out} versus I_{in}) characteristics are invaluable as a diagnostic tool. The exact form of these dynamical characteristics is a matter of experimental and computational convenience. In figure 3(a) we show a particularly useful form. In this figure we present a set of what can be termed 'equal-amplitude' experimental characteristics plotted for a niobium

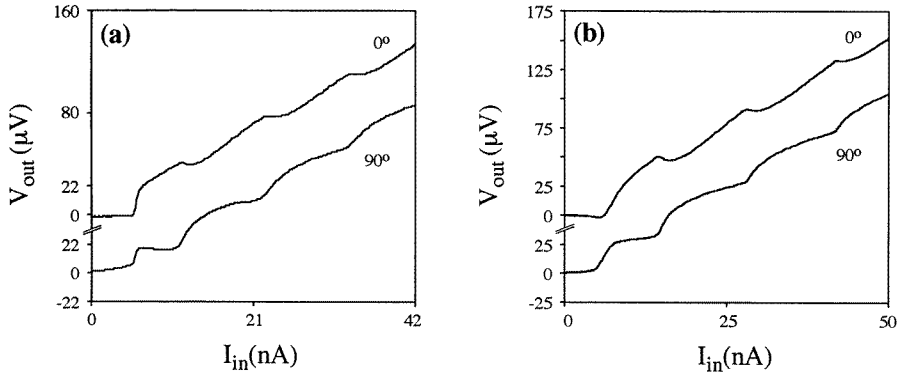

Figure 3. (a) Experimental equal-amplitude dynamical characteristics (V_{out} versus I_{in}) for a niobium point contact weak-link–rf-tank-circuit system recorded at 4.2 K. (b) Best-fit equal-amplitude characteristics for the ring screening current computed from the ground-state ($\kappa = 0$) energy of figure 1.

point contact ring–tank-circuit system operated at 4.2 K. Here, the system is driven, as is traditional, at the resonant frequency of the bare tank circuit ($f_R = \omega_R/2\pi$) and the tank-circuit voltage V_{out} is rf phase-sensitive detected with respect to the drive current I_{in}. Of course, it is perfectly practicable to find the two components of V_{out} which are precisely at 0° and 90° relative to I_{in}. However, these components are usually very different in magnitude. It is often far better to plot the equal-amplitude characteristics in which these two components are strictly comparable, as is evident in figure 3(a). In practice, the equal-amplitude characteristics are found by maintaining the phase difference at 90° between the components V_{out}^x and V_{out}^y, whilst the phase of both relative to the coherent forcing term I_{in} is rotated until the average slopes of the dynamical characteristics are the same at large I_{in}.

Theoretically, the equal-amplitude characteristics can be found by solving the non-linear equation of motion (2.5) for the coupled quantum–classical system. Knowing Λ, μ, L_t, C_t, R_t, Q and the system noise temperature T_N, we can best fit by computation to the experimental characteristics by a judicious choice of the form of the ground-state screening current $\langle I_s(\Phi_x)\rangle_0$ and of the effective weak-link capacitance C. From our previous arguments we choose this capacitance to be 10^{-16} F. We can then infer $\bar{h}\nu$ which, for the characteristics of figure 3(a), we find to be $0.06\Phi_0^2/\Lambda$. This value of $\bar{h}\nu$ corresponds to a weak-link critical current I_c ($=2e\nu$) of 2.5 μA. In this computer modelling we have included the rounding effect on these characteristics of a noise source with a noise temperature T_N of 4.2 K. Given the very weak coupling (i.e. small K^2) between the SQUID ring and the tank circuit (plus the following rf amplifier), it seems perfectly reasonable to take the effective noise temperature to be the ambient temperature (4.2 K) in our experiments. In figure 3(b) we show the computed equal-amplitude characteristics which best fit the experimental data of figure 3(a) with $\bar{h}\nu = 0.06\Phi_0^2/\Lambda$, $\Lambda = 3 \times 10^{-10}$ H and $T_N = 4.2$ K, where the screening current pattern corresponds to the ground-state energy $E_0(\Phi_x)$ in figure 1.

The small-amplitude dynamical response tells essentially the same story, but with more experimental resolution. In figures 4(a) and 4(b), respectively, we show the experimental $f_{r0}(\Phi_{xqstat})$ and $A_{r0}(\Phi_{xqstat})$ plots for the ring–tank-circuit system of figure 3, taken at 4.2 K in the absence of external em fields. Here, the coupling parameter is again $K^2 = 0.0016$ with a quality factor Q for the coupled system of 930 at a static bias flux $\Phi_{xqstat} = n\Phi_0$, n integer. The very accurately measured bare resonant frequency of the tank circuit (uncoupled from

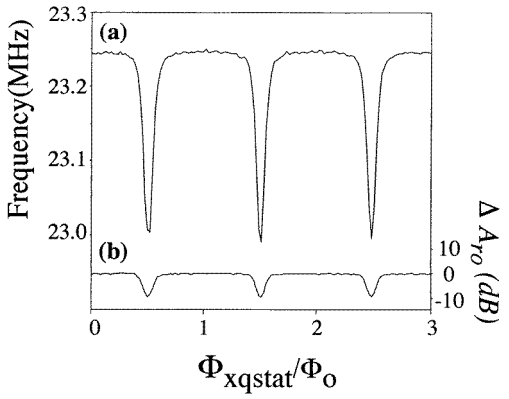

Figure 4. (a) The experimental peak frequency f_{r0} and (b) peak amplitude A_{r0}, of a coupled SQUID ring–rf-tank-circuit resonance as a function of Φ_{xqstat} for the system of figure 3 with no em field applied; here, $f_R = \omega_R/2\pi = 23.211$ MHz, $\varphi = \Phi_0/60$, $K^2 = 0.0016$, $Q = 930$ and $T = 4.2$ K.

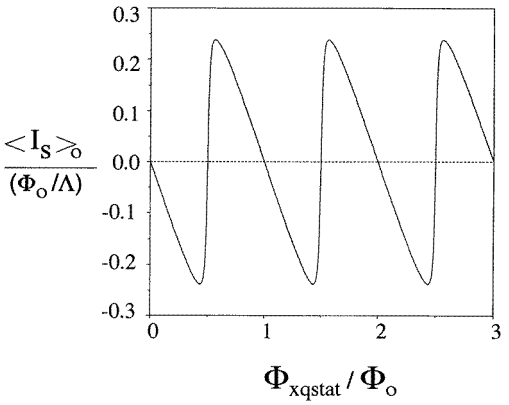

Figure 5. The best-fit ground-state ring screening current pattern $\langle I_s(\Phi_{xqstat})\rangle_0$ for the experimental frequency shift data of figure 4.

the SQUID ring) was 23.211 MHz and the rf signal level was $\Phi_0/60$. By inspection, it is apparent, via (2.6), that the ground-state screening current response $\langle I_s(\Phi_{xstat})\rangle_0$ of the SQUID ring is quite close to a sawtooth pattern, with a relatively small splitting at half-integer bias. Using the data of figure 4(a), and the ring–tank-circuit parameters of figure 3, we can best fit this response with $\overline{h}\nu = 0.06\Phi_0^2/\Lambda$. For $\Lambda = 3 \times 10^{-10}$ H and $C = 10^{-16}$ F this makes the minimum splitting frequency at $\Phi_{xqstat} = (n + 1/2)\Phi_0$, between the ground and first excited eigenenergies of the ring, equal to 219 GHz. The corresponding almost sawtooth screening current pattern is shown in figure 5.

We note that screening current patterns, Φ_0-periodic in the external flux, can also be generated from the quasi-classical description of the SQUID ring in which the ring is sited at or very close to the minimum in its potential as the flux is varied [20, 21]. Thus, the almost sawtooth pattern of figure 5, inferred from the ground-state solution of the TISE, would be close in functional form to that calculated quasi-classically in the (inductive) regime given that the parameter β $(=2\pi\Lambda I_{crit}/\Phi_0) \to 1$ from below. If only the ground states are

invoked, as is the case for the data reported in this paper, then, for very similar sawtooth screening current patterns ($I_s(\Phi_x)$), both the quasi-classical (i.e. the resistively shunted junction plus capacitance—the RSJ + C—model where the capacitance is large (typically $\approx 10^{-13}$ F for point contacts)) and quantum approaches will yield very similar small- (rf-) amplitude adiabatic modulation frequency shift patterns (see (2.9) and (2.12)). However, it must be remembered that in both the quantum and quasi-classical models the ring–tank-circuit system is highly non-linear in its dynamical behaviour—particularly so when $I_s(\Phi_x)$ is close to being a sawtooth. In the quasi-classical model the non-linear properties of the coupled system tend to act against the SQUID ring following the minimum in its potential adiabatically. This is strictly not the case for the quantum model provided that there is negligible superposition mixing in of higher states. Clearly, these non-linear effects will be minimized if the rf amplitude is made very small (in experiments $\mu\varphi \approx \Phi_0/100$), as is the case for the frequency shift patterns. By contrast, non-linear effects will be strong in the large-rf-amplitude ($\mu\varphi \approx$ a few Φ_0) regime required to observe SQUID magnetometer dynamical characteristics of the type shown in figure 3. It is here that the quantum and quasi-classical models differ strongly. In comparing the two models (with a tank circuit), the full non-linear RSJ + C approach will generate a given large-amplitude dynamical characteristic starting from a much more rounded out $I_s(\Phi_x)$ than is required to produce a very similar characteristic in the quantum model. This means that even if a reasonable fit can be made to large-rf-amplitude experimental data using the RSJ + C approach, no such fit can be made to the small-rf-amplitude dynamics where the computed frequency shift may be a factor of 5 or more smaller than that observed experimentally [22]. By comparison, given a close-to-sawtooth $I_s(\Phi_x)$ (which can be inferred from frequency shift data), the quantum model accurately reproduces both the small- and large-amplitude dynamics. Furthermore, in the presence of applied em fields of high enough frequency/amplitude, superposition mixing between the ground and first excited eigenstates occurs in the quantum description. In this case much richer frequency (and amplitude) shift structure can develop which cannot be generated in the quasi-classical model. As we have reported recently [9], we appear to have observed aspects of this rich structure at applied em frequencies and flux amplitudes at which, in the quantum description, non-adiabatic (pumped superposition mixing) behaviour should be observed. Though of obvious interest to our discussions, we emphasize that such non-adiabatic behaviour forms no part of the investigations described in this paper.

The minimum splitting frequency of 219 MHz is a first approximation. The presence of 4.2 K tank-circuit noise [17] means that the experimentally determined frequency response peak at around $\Phi_{xqstat} = (n + 1/2)\Phi_0$ is broadened. Hence, the underlying, and sharper, response in the absence of noise rounding corresponds to a smaller value of this minimum splitting frequency (and a slightly larger value of $\overline{h}\nu$). Thus, for particular values of Λ and C, and in the presence of 4.2 K noise originating in the (classical) tank circuit, we have solved the ring–tank-circuit equation of motion (2.5) to determine the best-fit value of $\overline{h}\nu$ which would yield the screening current pattern of figure 5. We found this to be $0.07\Phi_0^2/\Lambda$ with a corresponding minimum splitting at $\Phi_{xqstat} = (n + 1/2)\Phi_0$ of 144.6 GHz (2.07 mm free-space wavelength). We therefore infer that the noise-rounded data fitted by $\overline{h}\nu = 0.06\Phi_0^2/\Lambda$ (figure 5) are equivalent to an underlying $\overline{h}\nu = 0.07\Phi_0^2/\Lambda$. We note that the small-amplitude reactive technique is sufficiently sensitive to pick up on these small corrections in $\overline{h}\nu$.

In our quantum mechanical description of the SQUID ring we have made use of the simple (single-moded) lumped-component Hamiltonian (2.2). Now, in principle, a distributed circuit model would be preferred when considering the full dynamics of the ring. This subject has been discussed extensively by us in a recent series of articles [5,

13, 14]. However, this paper is only concerned with the properties of the ground state of the lowest-energy mode of the weak-link ring. The lowest-energy state is parametrized in terms of a few simple quantities (inductance, capacitance and critical current) which can be derived from the distributed circuit model [5].

We note that in computing the eigenenergies of the SQUID ring using the Hamiltonian (2.2), the parameter $1/\sqrt{\Lambda C}$ defines an energy scale, but does not define the resonant frequency of the SQUID block in the absence of the weak link. This parameter is related to the effective inductance and effective capacitance of the SQUID block, but the effective capacitance should also include a term which is dependent on the critical current of the weak link [5, 13, 14]. Hence, the natural resonant frequency of the block in the absence of the weak link will be different to the parametrization of the field energy ($\div h$) in the presence of a weak link.

There is one further point that should be made. With almost sawtooth screening current patterns, as is the case in the experiments described in this paper, the non-linearities which drive the adiabatic modulation of the SQUID ring are very close to half-integer bias flux ($\Phi_x = (n + 1/2)\Phi_0$) where the frequency separation ($\times h$) between the ground- and first-excited-state eigenenergies is a minimum. This is where there are significant superpositions of the quantized thick-ring flux states. By contrast, for almost sawtooth ground-state screening current patterns, the ring is essentially in a flux eigenstate at integer flux, $\Phi_{xstat} = n\Phi_0$. From this viewpoint we would therefore argue that it is the minimum splitting frequency at $\Phi_{xqstat} = (n + 1/2)\Phi_0$ that is relevant.

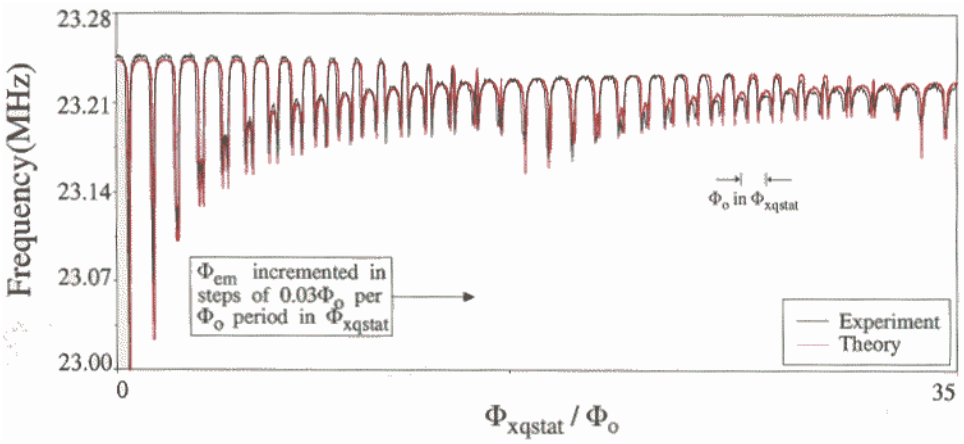

Figure 6. With the same experimental conditions and circuit parameters as in figure 4, the effect of monochromatic radiation at 290 MHz on the ground state $f_{r0}(\Phi_{xqstat})$, where Φ_{em} has been incremented in stages of $0.03\Phi_0$ at every Φ_0-increase in Φ_{xqstat}—shown in black. The adiabatically modulated $f_{r0}(\Phi_{xqstat})$ pattern computed using the best-fit $\langle I_s(\Phi_{xqstat})\rangle_0$ of figure 5, the circuit parameters of figure 4 and a Φ_{em} incremented in steps of $0.03\Phi_0$ from 0 to $1.04\Phi_0$—shown in red.

In any modelling of the modulation of a quantum mechanical SQUID ring by an external em field it is, of course, important to determine whether this involves just the ground state, or if this field is of high enough frequency and/or amplitude to mix in excited states of the ring. We can check this quantitatively by solving the TDSE for the system if we know the value of the minimum splitting frequency between the ground and first excited eigenenergies of the ring. In this situation we need only consider the effect of the em field

on the ground-state screening current. With this in mind, we show in black in figure 6(a) the effect of an external 290 MHz em field on the peak frequency and peak amplitude patterns of the ring–tank-circuit system of figures 3 and 4. Here, Φ_{em} was incremented in steps of $0.03\Phi_0$ every time Φ_{xqstat} reached an integer-flux state $n\Phi_0$, and $f_{r0}(\Phi_{xqstat})$ and $A_{r0}(\Phi_{xqstat})$ were then plotted over a complete Φ_0-period. This process was repeated many times to build up the dependence of these quantities on both Φ_{xqstat} and Φ_{em}. Experimentally, the modulating em field was fed to the SQUID ring by means of a weakly coupled microwave triplate-electrode structure [23] comprising the two, plane-parallel central sections of the two-hole SQUID ring with an insulated third strip electrode positioned between them. This scheme allowed for relatively broad-band coupling. The triplate electrode was fed via a 50 Ω microcoaxial cable connected to an external frequency synthesized source at room temperature. As can be seen, the effect of adiabatic em modulation, with incremented amplitude increases every Φ_0-period in Φ_{xqstat}, is to build up a very distinctive, Bessel-like frequency shift pattern. With an experimentally determined effective minimum splitting of 144.6 GHz (taking account of the 4.2 K noise present in the tank circuit), and with the $\kappa = 0$ and 1 eigenenergy structure $E_\kappa(\Phi_x)$ appropriate to the data of figure 4, we find that for an em frequency of 290 MHz there is absolutely negligible superposition mixing between these two states up to the end of the data run in figure 6 ($\Phi_{em} = 1.02\Phi_0$). We therefore used the ground-state screening current pattern of figure 5 (in the form of a look-up table) to compute the modulated current (2.9) and susceptibility (2.10).

For weak ring–em-field and ring–tank-circuit coupling this adiabatic modulation can be modelled very precisely in terms of equations (2.12), (2.9) and the frequency shift expression (2.6), provided that we know $\langle I_s(\Phi_x)\rangle_0$, Φ_{em} and K^2. In figure 6(b) we show in red the computed adiabatic modulation frequency shift pattern for the SQUID ring–tank-circuit system of figures 3 and 4 (with the best-fit screening current pattern (figure 5) sampled as a look-up table), where Φ_{em} has been incremented in steps of $0.03\Phi_0$ every Φ_0-period in Φ_{xstat} over an amplitude range of 0 to $1.04\Phi_0$ and f_R(measured) = 23.211 MHz. The correspondence between the theoretical and experimental modulation patterns of $f_{r0}(\Phi_{xstat})$ is quite apparent. We note that the data of figure 6(a) for SQUID rings with almost sawtooth screening current patterns (exemplified by figure 5) are totally typical of adiabatic modulation. In our experiments, with data taken on over one hundred such SQUID rings, these modulation patterns were always observed when the applied microwave frequency was small compared with the estimated frequency difference between the ground- and first-excited-state eigenenergies. In fact, this adiabatic modulation has been used by us to set the basis for, and contrast with, the onset of non-adiabatic (mixing between the ground and first excited eigenstates) at much higher frequencies [9].

As is clear from the screening current pattern of figure 5, the response of the SQUID ring to an external flux can be extremely non-linear. Taking just the case of the ring interacting with the time-dependent flux generated in a rf tank circuit, the back reaction of this current response on the tank circuit leads to distinctive non-linear phenomena. These have been the subject of several of our recent publications [17] and form part of a distinct branch of non-linear dynamics [24–26]. In particular, the whole of the resonance lineshape, both the peak frequency and peak amplitude, of a coupled ring–tank-circuit system depends on the static bias flux applied to the ring. This can be seen in the data of figure 4(b) where the peak amplitude A_{r0} is a strongly non-linear function of Φ_{xqstat}, with a minimum at the half-integer bias. It was consequently of considerable interest to try to determine the effect of changes in the strength of the coupling between the ring and the em field on the adiabatic modulation pattern. We therefore needed both to be able to adjust this coupling in a controlled manner and to measure its strength. This was achieved by following the

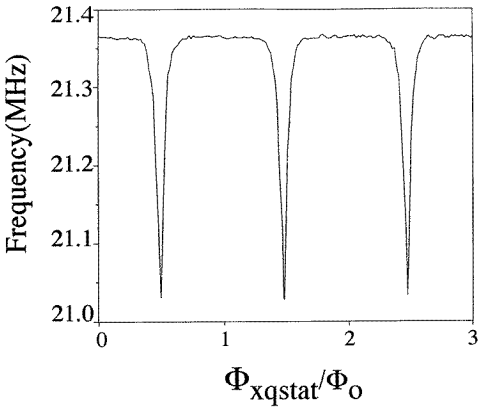

Figure 7. The experimental unmodulated frequency shift pattern $f_{r0}(\Phi_{xqstat})$ for a SQUID ring coupled to a tank circuit driven at 21.307 MHz with $K^2_{(rf)} = 0.0027$ and $T = 4.2$ K.

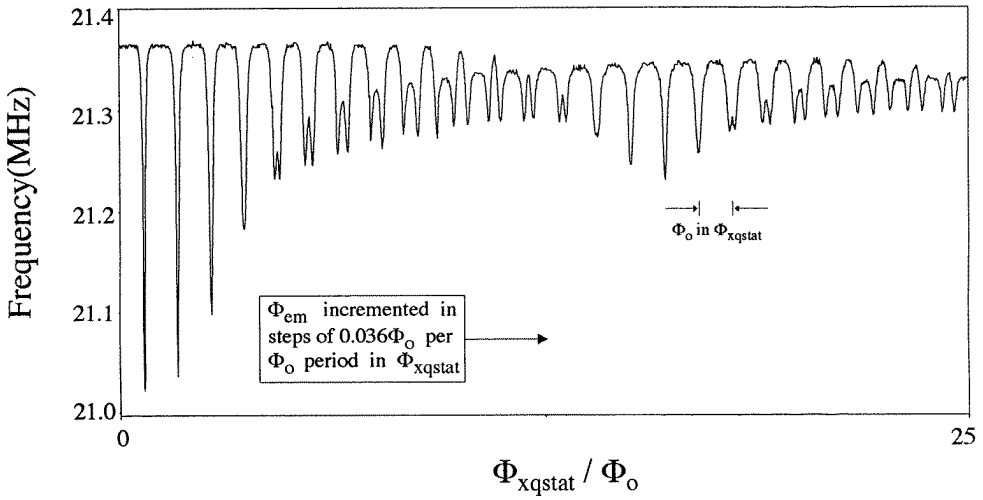

Figure 8. For the same system as for figure 7 the adiabatically modulated $f_{r0}(\Phi_{xqstat})$ for an em frequency of 330 MHz fed through a uhf tank circuit resonant at 330 MHz. Here, $K^2_{uhf} \cong 0.001$ and the the rf probe frequency is 21.307 MHz at an amplitude of $\varphi = \Phi_0/60$, with again $K^2_{(rf)} = 0.0027$ and $T = 4.2$ K.

procedure already adopted at rf, i.e. a tuned coil was introduced into the second hole of the niobium SQUID, this time resonant at uhf (330 MHz). As with the resonant rf probe circuit, the coupling of the uhf circuit, acting adiabatically on the SQUID ring, could be changed by moving its coil with respect to the hole in the SQUID ring. In figure 7 we show the unmodulated ground-state frequency shift pattern for this second experimental SQUID ring which contained both the tuned rf and uhf coils. Conveniently for our purposes in this paper, the screening current response $\langle I_s(\Phi_x)\rangle_0$ for this SQUID ring is very close to that of figure 5. In figure 8 the effect of adiabatically modulating the SQUID ring, i.e. $f_{r0}(\Phi_{xqstat})$, with uhf (330 MHz) is shown. Here, the coupling between the ring and the external em field is weak ($K^2_{uhf} \cong 0.001$) (as for figure 6), as is the rf probe signal ($\varphi = \Phi_0/60$). Clearly, the modulation pattern of figure 8 is strictly comparable with that shown in figure 6(a). In figure 9 the adiabatically modulated $f_{r0}(\Phi_{xqstat})$, equivalent to figure 8, but now for much stronger uhf coupling strength ($K^2_{uhf} \cong 0.03$), is shown. Here, it is apparent that the non-

linear behaviour of $\langle I_s(\Phi_x)\rangle_0$ around $\Phi_x = (n + 1/2)\Phi_0$ has led to a change in $f_{r0}(\Phi_{xqstat})$. Clearly, the very strong non-linear dynamical behaviour of the coupled system close to half-integer bias has led to the reduction in the level of uhf impinging on the SQUID ring in an exactly analogous way to that already observed at rf (see figure 4(b)). In turn, this has led to the loss of the distinctive splitting feature found at small Φ_{em}-amplitudes which is quite apparent in figures 6(a) and 6(b) and figure 8.

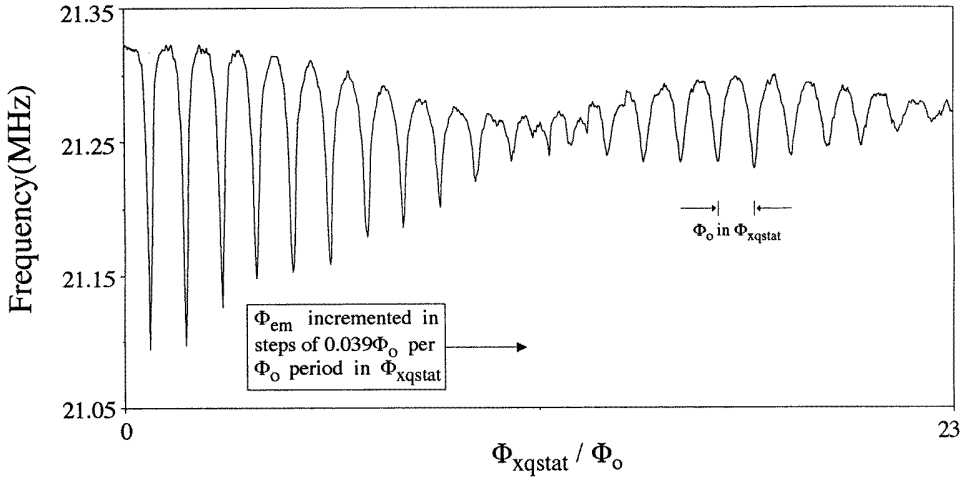

Figure 9. As for figure 8, with the same adiabatic modulation frequency (330 MHz) but now with $K^2_{uhf} \cong 0.03$, again at $T = 4.2$ K.

For the strongly coupled case, the reduction of the uhf power level impinging on the SQUID ring, due to non-linear effects, can be modelled successfully by solving the ring–uhf-resonator equation of motion analogous to (2.5) with the appropriate circuit parameters. As an illustration, we present in figure 10 a computed example in which the ring (using the screening current pattern $\langle I_s(\Phi_x)\rangle_0$ of figure 5) is coupled to a 200 MHz resonator. In figure 10(a) we show the actual uhf power impinging on the ring as a function of Φ_{xqstat} when the external power is incremented in steps of $0.05\Phi_0$; these increments appear as vertical discontinuities. For each external uhf power level, Φ_{xqstat} has been swept through one flux quantum, centred on $\Phi_0/2$. In figure 10(b) the half-integer power dips of figure 10(a) have been invoked to calculate the theoretical frequency shifts $f_{r0}(\Phi_{xqstat})$, using the screening current pattern of figure 5. This frequency shift pattern compares well with the form of the experimental data shown in figure 9.

Again, as with the modelling of the adiabatic modulation data of figure 6, and given that the small splitting screening current pattern relevant to the data in this figure is essentially the same (i.e. essentially the same $\kappa = 0$ and 1 eigenenergies $E_\kappa(\Phi_x)$ in the quantum model of the SQUID ring), we can solve the system TDSE. We find, once again, that there is negligible superposition mixing between the ground and first excited states at the em frequencies of 330 MHz up to the end of the data runs in figures 8 and 9. Thus, for the experimental data presented in figures 8 and 9 we need only consider the modulation of the ground state by the em field.

It is clear from a comparison of the experimental data, and the computed adiabatic responses of a SQUID ring to electromagnetic radiation, that the functional form of the screening current pattern (calculated from the quantum model of the ring), combined with

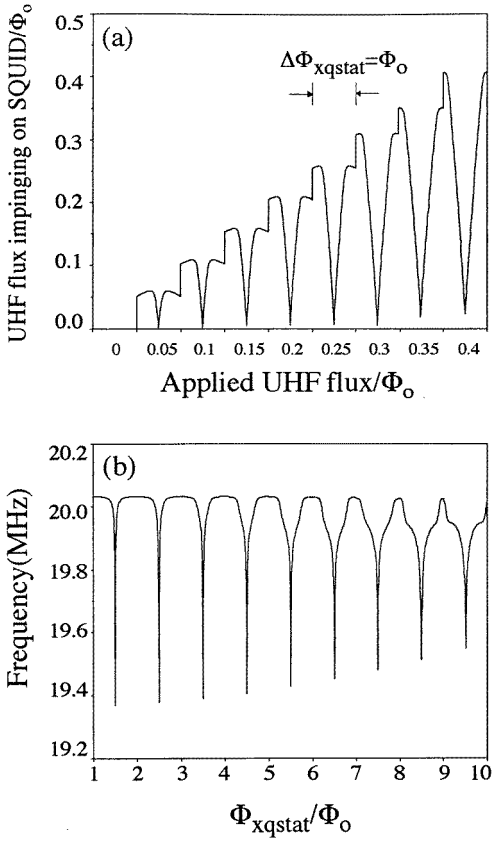

Figure 10. (a) The computed actual power impinging on the SQUID ring as a function of Φ_{xqstat} with the external power being incremented in steps of $0.05\Phi_0$; for each external power level Φ_{xqstat} is swept through one flux quantum centred on $\Phi_0/2$. The vertical jumps in this figure are where the external power has been incremented in steps of $0.05\Phi_0$. (b) The theoretical frequency shift pattern $f_{r0}(\Phi_{xqstat})$ calculated using the half-integer (i.e. at $\Phi_{xqstat} = (n+1/2)\Phi_0$, n integer) power dips shown in figure 10(a).

the non-linear equation of motion (2.5), provides a powerful and quantitative description of the coupled ring–tank-circuit system in the adiabatic regime.

Acknowledgment

We would like to thank the Engineering and Physical Sciences Research Council for its generous support of this work.

Appendix

As has been discussed at some length in the main part of this paper, the frequency shift technique allows us to monitor the change in the resonant frequency of the rf tank circuit coupled to the SQUID ring, and hence the magnetic susceptibility χ_κ of the ring, as a function of the quasi-static bias flux Φ_{xqstat}. With the application of an em field of much

higher frequency than that of the very-small-amplitude rf probe signal to the SQUID ring, χ_κ becomes a function of both the quasi-static and em components of the applied magnetic flux. The SQUID ring, with an estimated minimum splitting frequency close to 200 GHz at $\Phi_x = (n + 1/2)\Phi_0$, can clearly follow the oscillations in the external em field, with the ring screening current and susceptibility varying concomitantly. However, the tank circuit, with a resonant frequency of around 20 MHz, cannot respond in real time to such rapid changes in the susceptibility and therefore 'sees' an average value. Since the em field applied to the SQUID ring is sinusoidally time dependent, the average is not equally balanced. Indeed, since more time is spent near the maximum excursions in the em flux amplitude than elsewhere in its cycle, the values of the ring susceptibility in these regions contribute disproportionally to this average.

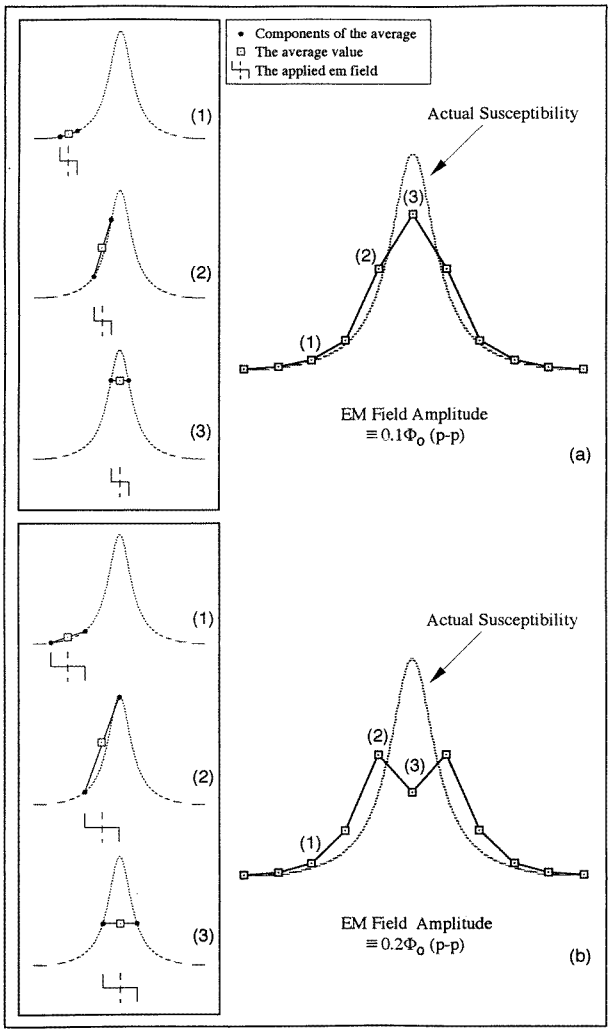

Figure A1. A graphical representation of the adiabatic modulation showing the effect of microwaves (approximated by a square wave) on the ring magnetic susceptibility for microwave flux amplitudes of (a) $0.1\Phi_0$ and (b) $0.2\Phi_0$, both peak to peak.

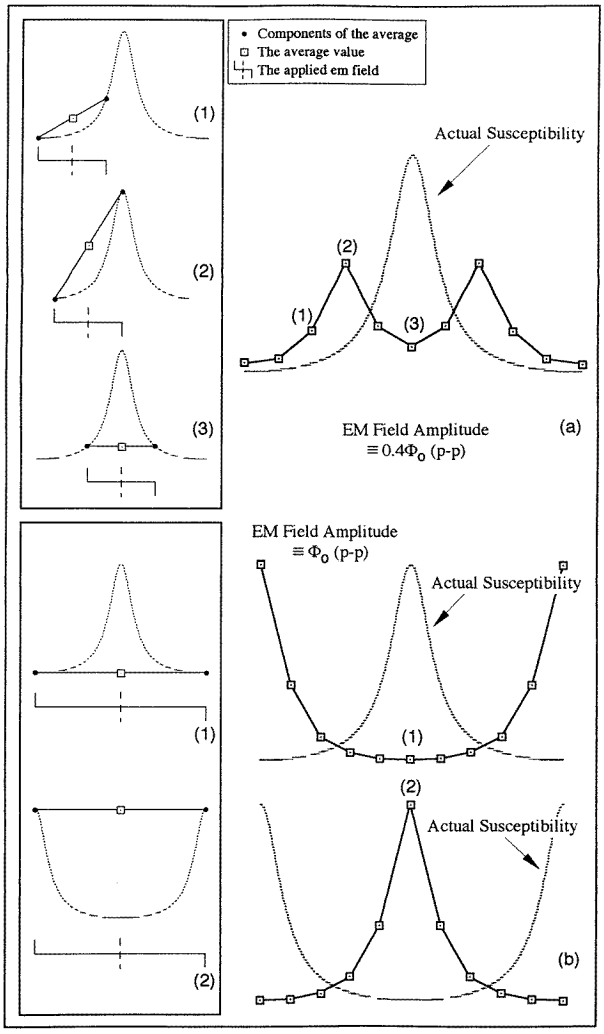

Figure A2. As for figure A1, with the microwaves approximated by a square wave, but with microwave flux amplitudes of (a) $0.4\Phi_0$ and (b) $1\Phi_0$.

It is possible to demonstrate this weighted effect on the average susceptibility which is monitored at rf simply by approximating the sinusoidal em oscillation by a square wave so that the maximum excursions (plus and minus) are occupied for the whole cycle. In figures A1 and A2 we illustrate graphically how the average value of the susceptibility arises. It can be seen that as the em flux amplitude is increased, the average susceptibility at the half-integer bias flux ($\Phi_{\mathrm{xqstat}} = (n + 1/2)\Phi_0$) becomes progressively lower than the actual susceptibility. At sufficiently large em amplitudes, the nature of the weighting causes the average susceptibility at the half-integer bias to fall below the average value on either side. The effect of this is to generate a second feature. When the em flux amplitude is increased to Φ_0, peak to peak (figure A2(b)), the average susceptibility recovers the periodicity of the actual susceptibility but the functional form is shifted by $\Phi_0/2$ in Φ_{xqstat}. In the case of this simple square-wave example of adiabatic modulation, the maximum value of the

susceptibility is also recovered. However, when the microwave waveform is sinusoidal in time, the average is obviously not set completely by the value of the susceptibility at the peak excursions in amplitude of the em cycle. It follows that for sinusoidal microwave modulation, the maximum average susceptibility is always slightly less than the maximum in the actual susceptibility.

References

[1] Spiller T P, Clark T D, Prance R J and Widom A 1992 *Progress in Low Temperature Physics* vol XIII, ed D F Brewer (Amsterdam: Elsevier) p 219

[2] Widom A and Srivastava Y N 1987 *Phys. Rep.* **148** 1

[3] Aharanov Y and Vaidman L 1993 *Phys. Lett.* **178A** 38

[4] Viola L, Onofrio R and Calarco T 1997 *Phys. Lett.* **229A** 23

[5] Ralph J F, Clark T D, Prance R J and Prance H 1996 *Phys. Lett.* **220A** 30

[6] For quantum-optical analogues of the time-dependent SQUID problem considered in this paper, see, for example,
Cohen-Tannoudji C, Dupont-Roc J and Grynberg G 1992 *Atom–Photon Interactions* (New York: Wiley) chs II and VI

[7] Diggins J, Whiteman R, Clark T D, Prance R J, Prance H, Ralph J F, Widom A and Srivastava Y N 1997 *Physica* B **233** 8

[8] Clark T D, Diggins J, Ralph J F, Everitt M, Prance R J, Prance H and Whiteman R 1998 Coherent evolution and quantum transitions in a two-level model of a SQUID ring *Ann. Phys., NY* **268** 1–30

[9] Whiteman R, Clark T D, Prance R J, Prance H, Schöllmann V, Ralph J F, Everitt M and Diggins J 1998 *J. Mod. Opt.* **45** 1175

[10] See, for example,
Prance R J, Clark T D, Whiteman R, Diggins J, Ralph J F, Prance H, Spiller T P, Widom A and Srivastava Y N 1994 *Physica* B **203** 381
for an earlier discussion of the rf reactive technique.

[11] Ralph J F, Clark T D, Prance R J and Prance H 1996 *Physica* B **226** 355

[12] Zimmerman J E, Thiene P and Harding J T 1970 *J. Appl. Phys.* **41** 1572

[13] Ralph J F, Clark T D, Prance R J, Prance H and Diggins J 1996 *J. Phys.: Condens. Matter* **8** 10 753

[14] Ralph J F, Clark T D, Diggins J, Prance R J, Prance H and Widom A 1997 *J. Phys.: Condens. Matter* **9** 8275

[15] Prance H, Clark T D, Prance R J, Spiller T P, Diggins J and Ralph J F 1993 *Nucl. Phys.* B **33** 35

[16] Grover F W 1962 *Inductance Calculations, Working Formulas and Tables* (New York: Dover) p 142

[17] Clark T D, Ralph J F, Prance R J, Prance H, Diggins J and Whiteman R 1998 *Phys. Rev.* E **57** 4035

[18] Cohen-Tannoudji C, Diu B and Lalöe F 1997 *Quantum Mechanics* vol I (New York: Wiley) p 308

[19] National Instruments LabVIEW Software, 6504 Bridgepoint Parkway, Austin, TX 78730-5039, USA

[20] See
Barone A and Paterno G 1982 *Physics and Applications of the Josephson Effect* (New York: Wiley) ch 13 for a general discussion of frequency shift phenomena in the inductive regime of SQUID behaviour.

[21] Gallop J C 1991 *SQUIDS, the Josephson Effects and Superconducting Electronics* (Bristol: Hilger)

[22] Schöllmann V, Whiteman R, Clark T D, Everitt M, Prance H, Prance R J and Ralph J F 1998 Non-linear dynamical modelling of a SQUID ring–tank-circuit system in the inductive mode regime of behaviour, in preparation

[23] Edwards T 1992 *Foundations for Microstrip Circuit Design* (Chichester: Wiley) p 2

[24] Thompson J M T and Stewart H B 1986 *Non-linear Dynamics and Chaos* (New York: Wiley)

[25] Jordan D W and Smith P 1997 *Non-linear Ordinary Differential Equations (Oxford Applied Mathematics and Computing Science Series)* ed J Crank, H G Martin and D M Melluish (Oxford: Clarendon)

[26] Likharev K K 1986 *Dynamics of Josephson Junctions and Circuits* (Sidney: Gordon and Breach) pp 490–4